Dynamic Mobile Manipulation via Whole-Body Bilateral Teleoperation of a Wheeled Humanoid

Amartya Purushottam, *Graduate Student Member, IEEE*, Christopher Xu, Yeongtae Jung, *Member, IEEE*, and Joao Ramos

***Abstract*—Humanoid robots have the potential to help human workers by realizing physically demanding manipulation tasks such as moving large boxes within warehouses. We define such tasks as Dynamic Mobile Manipulation (DMM). This letter presents a framework for DMM via whole-body teleoperation, built upon three key contributions: Firstly, a teleoperation framework employing a Human Machine Interface (HMI) and a bi-wheeled humanoid, SATYRR, is proposed. Secondly, the study introduces a dynamic locomotion mapping, utilizing human-robot reduced order models, and a kinematic retargeting strategy for manipulation tasks. Additionally, the letter discusses the role of whole-body haptic feedback for wheeled humanoid control. Finally, the system's effectiveness and mappings for DMM are validated through locomanipulation experiments and heavy box pushing tasks. Here we show two forms of DMM: grasping a target moving at an average speed of 0.4 m/s, and pushing boxes weighing up to 105% of the robot's weight. By simultaneously adjusting their pitch and using their arms, the pilot adjusts the robot pose to apply larger contact forces and move a heavy box at a constant velocity of 0.2 m/s.**

***Index Terms*—Humanoid whole-body control, telerobotics and teleoperation, human and humanoid motion analysis and synthesis, human-in-the-loop, motion retargeting.**

I. Introduction

CARGO, freight, and heavy-lift accidents are common occurrences in the maritime, transportation, and warehousing industries. While manually slotting cargo containers on ships, workers are at risk of injuring their backs and being hurt by loose cargo that may be set in motion due to the rocking of the boat. With growing safety and labor concerns, humanoid robots are a potential solution that demands exploration. To be effective tools, they must be capable of Dynamic Mobile Manipulation (**DMM**): simultaneous coordination of locomotion and manipulation to accomplish a forceful physical task that cannot be realized semi-statically. For instance, the robot cannot move a large box without intentionally falling towards it. Humans exhibit DMM when they use their upper and lower body to regulate contact forces and accelerations of a box that would otherwise be too heavy to push with their arms alone. Such online planning of whole-body capabilities have yet to be seen on robotic platforms even after decades of incredible progress in perception, planning, and control within the robotics community. Teleoperation presents a promising opportunity for bridging this gap between human sensorimotor skills and autonomous control by integrating human planning into robot control loops. By leveraging human whole-body planning and intuition of force interactions with the environment, robots may become more capable at DMM tasks.

One approach to transporting complex human whole-body control and force regulation to humanoids is to create an immersive experience where the robot behaves as an extension of the human via motion similarity and retargeting strategies [1], [2]. This way we can utilize the operator's body motion—captured in real-time—to generate poses and trajectories that the robot can follow. More specifically, to enable hands-free teleoperated [3] DMM, we envision that the robot arms will track the motion of the operator's arms for manipulation while locomotion of the robot's base will be controlled by the operator's body lean. To provide the pilot information about the robot's surroundings and further the immersive experience, we deliver haptic feedback to the human to allow them to feel similar forces to those experienced by the robot. This bilateral teleoperation framework - where the pilot sends commands and receives sensory feedback from the robot - has been shown to be effective in transferring human motion control for humanoid telelocomotion [4].

In this work, we capture the human arm motion through an upper body exoskeleton frame, as well as the human center of mass (**CoM**), center of pressure (**CoP**), and head orientation through the Human Machine Interface (**HMI**) [5]. Feedback forces up to 155 N along the sagittal plane are delivered through the HMI's two linear actuators to the pilot's vest. The HMI communication with the robot controllers runs at 500 Hz. As such, we do not explicitly study time delays in this work but refer readers to [6], [7] for studying instability due to delays and slow updates rates.

Manuscript received 3 July 2023; accepted 28 October 2023. Date of publication 20 November 2023; date of current version 26 December 2023. This letter was recommended for publication by Associate Editor T. Hulin and Editor J.-H. Ryu upon evaluation of the reviewers' comments. This work was supported by the National Science Foundation under Grant IIS-2024775. *(Corresponding author: Amartya Purushottam.)*

This work involved human subjects or animals in its research. Approval of all ethical and experimental procedures and protocols was granted by the University of Illinois Urbana-Champaign.

Amartya Purushottam and Christopher Xu are with the Department of Electrical and Computer Engineering, University of Illinois Urbana-Champaign, Champaign, IL 61820 USA (e-mail: purusho2@illinois.edu; cyx3@illinois.edu).

Yeongtae Jung is with the Department of Mechanical System Engineering and Advanced Transportation Machinery Research Center, Jeonbuk National University, Jeollabuk-do 54896, Republic of Korea (e-mail: ytjung@jbnu.ac.kr).

Joao Ramos is with the Department of Electrical and Computer Engineering, University of Illinois Urbana-Champaign, Champaign, IL 61820 USA, and also with the Department of Mechanical Science and Engineering, University of Illinois Urbana-Champaign, Champaign, IL 61820 USA (e-mail: jlramos@illinois.edu).

Digital Object Identifier 10.1109/LRA.2023.3334677

The primary contributions of this study are:

- Development of a model-based dynamic locomotion mapping using human-robot Reduced Order Models (**RoM**) and a kinematic manipulation retargeting strategy
- Formulation of a haptic feedback law that gives the pilot increased pitching range of motion and enables them to feel robot external forces during manipulation for an improved immersive experience
- Experimental validation of our whole-body teleoperation framework for DMM in the context of heavy (105% robot weight and unknown to pilot) box pushing.

II. Related Work

Researchers have addressed the locomotion and manipulation of humanoids by developing controllers using full-body dynamics [8], [9], or reduced-order models such as the Wheeled Inverted Pendulum (**WIP**) [3], [10], and Linear Inverted Pendulum (**LIP**) [5], [11]. However, these works did not demonstrate upper and lower body coordination to manipulate the robot's surroundings - a prerequisite of DMM. Minniti et al. in [12] showcased impressive dexterity and interaction in performing mobile manipulation tasks with their balbot manipulator, using model predictive control and an adaptive parameter estimator to open doors and lift objects. Stillman et al. presented the Golem Krang [13], a bi-wheeled manipulator capable of balancing while performing heavy lifting. Other related works [14] have integrated vision pipelines to facilitate mobility and manipulation. While these studies show promising preliminary forms of DMM, they do do not leverage human adaptability, and are constrained in their capacity to modify the robot's posture to synergistically combine the robot's body and arms for force amplification. Recently, researchers proposed a framework that generates poses offline for heavy box pushing experiments, utilizing the robot's inertia and arm manipulation for DMM [15]. The authors here rely on significant assumptions about knowledge of the environment (object mass, inertia, global pose, etc.) and require offline pose optimization prior to execution.

Teleoperated systems offer a solution to the aforementioned challenge of offline trajectory and pose generation by utilizing human intuition and planning. Previous works have demonstrated mobile manipulation through whole-body teleoperation [16], [17]. These systems, however, are constrained by predefined switching modes for locomotion and manipulation or limited control over individual sections of the robot. Such motion retargeting strategies restrict the dynamic capabilities of these platforms. Although real-time whole-body motion retargeting strategies from humans to humanoids have been proposed [1], [18], they have only been explored in simulation or for statically stable robots.

Moreover, physical differences between humans and robots, such as size and mass, make it challenging to create direct, one-to-one mappings between human and robot movements. Researchers have explored the use of whole-body haptic feedback [4], [11], [19] to bridge this gap between human and robot dynamics. These studies and our previous work [3], [5] did not explicitly convey the robot's environment interaction forces back to the pilot, and have yet to show its effect on the human's feedback force.

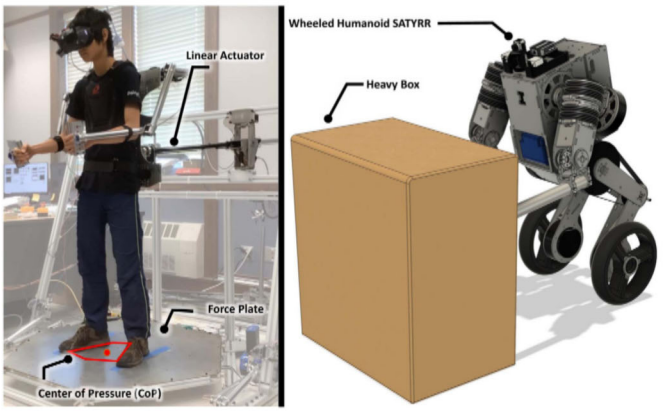

Fig. 1. Dynamic mobile manipulation: The pilot in the HMI (left) teleoperates SATYRR (right) to push a heavy box of unknown mass. Linear actuators deliver haptic feedback to human torso informing them of the robot-environment interaction forces. Supplementary video: https://youtu.be/QqcJsSH0YjY.

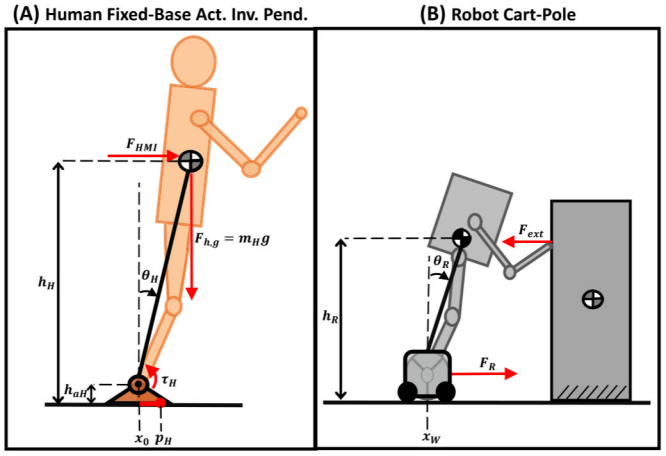

Fig. 2. (a) The human is modeled as an actuated pendulum where the ankle as treated as an actuator to control lean. (b) The robot is modeled as a cart-pole for generating desired references.

III. Background

Retargeting of individual limbs and whole-body movements is challenging due to human-robot kinematic differences [18], and the increased computational cost associated with controlling larger nonlinear models. Therefore, we use RoM that reduce modeling complexity while still capturing the key unstable dynamics of the robot and human. The human's arms and body motion are used to generate retargeted trajectories, eliminating the need for a joystick in this hands-free teleoperation framework [3]. Using body pitch, as shown in Fig. 2, the pilot can directly control interaction forces between the robot and its environment.

Here, we briefly revisit the robot cart-pole RoM used for mappings, and the human Divergent Component of Motion (**DCM**) that captures their dynamic balancing strategy.

A. Cart-Pole Model

The dynamics of the cart-pole system, linearized around the upright zero position $(\sin(\theta_R) \approx \theta_R;\ \cos(\theta_R) \approx 1)$, with small

pendulum velocities ($\dot{\theta}_R^2 \approx 0$) can be written in state-space form [20]:

$$\begin{bmatrix} \dot{x}_w \\ \ddot{x}_w \\ \dot{\theta}_R \\ \ddot{\theta}_R \end{bmatrix} = \begin{bmatrix} 0 & 1 & 0 & 0 \\ 0 & 0 & -\frac{m}{M}g & 0 \\ 0 & 0 & 0 & 1 \\ 0 & 0 & \frac{mg}{Mh_R} & 0 \end{bmatrix} \begin{bmatrix} x_w \\ \dot{x}_w \\ \theta_R \\ \dot{\theta}_R \end{bmatrix} + \begin{bmatrix} 0 \\ \frac{1}{M} \\ 0 \\ \frac{-1}{Mh_R} \end{bmatrix} u + \begin{bmatrix} 0 \\ 0 \\ 0 \\ \frac{1}{mh_R} \end{bmatrix} F_{ext} \tag{1}$$

where x_w represents the horizontal position of the cart, θ_R the angle between the cart and CoM, h_R the pendulum height, g the gravity constant, u the force applied to the cart, and F_{ext} a disturbance force applied at the CoM as seen in Fig. 2. The mass of the cart base, M, for humanoid robots can assumed to significantly smaller than the the mass of the body, m. In other words, $m \gg M$.

Here, it can be seen that controlling desired base acceleration is proportional to controlling the robot's lean angle: $\ddot{x}_w^{des} \propto \theta_R^{des}$. In other words, the pilot can control translational forces exerted on the environment by the robot through regulation of the robot's pitch.

B. Divergent Component of Motion (DCM)

Human motion for balancing and locomotion can be captured by pendular systems such as the LIP. The pendular DCM is the unstable component of the dynamics that we assume also captures the human's balancing strategy [21]. Specifically, human motion can be stabilized as long as the LIP DCM remains within the human support polygon: $p_x^{\min} \leq x_o + \frac{\dot{x}_o}{\omega_o} \leq p_x^{\max}$. Here, x_o is the CoM horizontal position, $\omega_o = \sqrt{g/h}$ the human pendulum's natural frequency at height h under a gravity field g, and $p_x^{\min}, p_x^{\max}$ are the CoP minimum-maximum given by the human foot length. Under a change of state, $\theta_o = x_o/h$ (valid around the linearized zero position), this condition can be rewritten:

$$\frac{p_x^{\min}}{h} \leq \theta_o + \frac{\dot{\theta}_o}{\omega_o} \leq \frac{p_x^{\max}}{h} \tag{2}$$

We refer to the dimensionless pendular DCM as $\xi = \theta_o + \frac{\dot{\theta}_o}{\omega_o}$. For brevity, ξ will simply be referred to as the DCM.

IV. Kinodynamic Whole-Body Motion Retargeting

Here, we introduce the whole-body bilateral teleoperation mappings for DMM. The lower body telelocomotion mapping models the human and robot as pendulum systems along the sagittal plane. Section IV-A motivates the human fixed-base actuated inverted pendulum (**AIP**) model. Section IV-B defines a condition for stabilizing the robot cart-pole given by its dimensionless DCM. We use the human's dynamic balancing strategy given by their DCM and CoP to generate tracking references and haptic feedback as shown in Sections IV-C and IV-D. The upper body telemanipulation mapping outlined in Section IV-E uses similarity in human-robot arm joint topology to enable intuitive kinematic arm control. The focus lies on performing DMM through the proposed mappings and feedback, and does not necessarily claim exclusivity. The pilot's adaptability to different mappings and feedback present a challenge in establishing necessity within this context.

A. Human Motion Model

Use of human pitch for hands-free teleoperation and control of wheeled humanoids has shown viability [3]. Attempting to capture the pitch angle from classically used human locomotion models, such as the LIP, presents a problem however. This angle - defined between the human CoP and CoM - converges to zero in steady state as the CoP tracks the CoM ($p_H \rightarrow x_H$). This results in stop-and-go motions and unintuitive pitch control on wheeled robots. For example, the human may lean at a constant angle, but the desired reference is zero causing the robot be upright.

Thus, we propose applying a transformation to model the human as a fixed-base AIP as shown in Fig. 2. This allows us to define the pitch angle between the fixed human ankle and their CoM. This measurement remains constant in steady state and does not change as a function of the CoP. Instead, the CoP is used to define the ankle torque needed to stabilize the human inverted pendulum.

The dynamics for the AIP are given by:

$$\ddot{\theta}_H = \frac{g\sin(\theta_H)}{\tilde{h}_H} + \frac{1}{m_H \tilde{h}_H^2}\tau_H + \frac{\cos(\theta_H)}{m_H \tilde{h}_H} F_{HMI} \tag{3}$$

where m_H is the human's mass, and $\tilde{h}_H = h_H - h_{aH}$ is the difference in the CoM height, h_H, and ankle height, h_{aH}. The human pitch angle, θ_H, and human ankle torque, τ_H, are defined in the clockwise direction. The external feedback force, F_{HMI}, is applied to the human torso near their CoM. Human motion is measured and force feedback is applied in real time through this HMI [3], [5].

Linearizing around the $\theta_H = 0$ upright position, and assuming $h_H \gg h_{aH}$ allows us to write in state-space form:

$$\begin{bmatrix} \dot{\theta}_H \\ \ddot{\theta}_H \end{bmatrix} = \begin{bmatrix} 0 & 1 \\ \omega_H^2 & 0 \end{bmatrix} \begin{bmatrix} \theta_H \\ \dot{\theta}_H \end{bmatrix} + \begin{bmatrix} 0 \\ \frac{1}{m_H h_H^2} \end{bmatrix} \tau_H + \begin{bmatrix} 0 \\ \frac{1}{m_H h_H} \end{bmatrix} F_{HMI} \tag{4}$$

The state transition matrix has eigenvalues $\pm\omega_H$. Diagonalizing as shown in [22] and substituting human actuation as a function of their CoP ($\tau_H = -p_H m_H g$) we find the unitless divergent component of motions and its time derivative:

$$\xi_H = \theta_H + \tfrac{1}{\omega_H}\dot{\theta}_H \tag{5}$$

$$\dot{\xi}_H = \omega_H \xi_H - \tfrac{\omega_H}{h_H} p_H \tag{6}$$

B. Robot Cart-Pole DCM

To track the human pendular DCM we isolate the linearized cart-pole DCM here. The eigenvalues of (1) are: $(\lambda_{x_w}, \lambda_{\dot{x}_w}, \lambda_{\theta_R}, \lambda_{\dot{\theta}_R}) = (0, 0, \sqrt{g/h_R}, -\sqrt{g/h_R})$. The states corresponding to eigenvalues equal to 0 indicate marginally stable behavior in these modes. In other words, these states neither grow nor decay when perturbed. To design control references that can stabilize the unstable dynamics we focus on isolating the non-zero eigenvalue variables θ_R, and $\dot{\theta}_R$:

$$\begin{bmatrix} \dot{\theta}_R \\ \ddot{\theta}_R \end{bmatrix} = \begin{bmatrix} 0 & 1 \\ \alpha^2\omega_R^2 & 0 \end{bmatrix} \begin{bmatrix} \theta_R \\ \dot{\theta}_R \end{bmatrix} + \begin{bmatrix} 0 \\ \frac{-1}{Mh_R} \end{bmatrix} F_R + \begin{bmatrix} 0 \\ \frac{1}{mh_R} \end{bmatrix} F_{ext} \tag{7}$$

where $\omega_R = \sqrt{g/h_R}$ is the robot linear natural frequency and $\alpha = \sqrt{m/M}$ is a unitless quantity from (1).

Performing the same diagonalization and decomposition as in the previous section, letting $\omega_R^\circ = \alpha\omega_R$ (since α is unitless), we find the cart-pole DCM and its dynamics:

$$\xi_R = \theta_R + \tfrac{1}{\omega_R^\circ}\dot{\theta}_R \tag{8}$$

$$\dot{\xi}_R = \omega_R^\circ \xi_R - \tfrac{1}{\omega_R^\circ M h_R} F_R + \tfrac{1}{\omega_R^\circ m h_R} F_{ext} \tag{9}$$

C. Dynamic Locomotion Retargeting

The proposed tele-locomotion mapping accounts for the different sizes of the robot and human by normalizing along their natural frequency, masses, and heights [4]. The tracking of the DCM is a design choice in this framework motivated by its ability to capture the dynamic balancing requirement of the human pendulum model. By enforcing the robot to follow the human's DCM and its time derivative we can:

- Stabilize and dynamically control the robot using the AIP DCM as a tracking reference
- Capture the non-minimum phase behavior of the human CoP as a feedforward for increased responsiveness
- Explicitly model and map virtual and external forces acting on the human and robot

We choose the DCM as our retargeted state and aim to achieve:

$$\xi_R = \xi_H \tag{10}$$

To minimize the DCM error, $|\xi_R - \xi_H|$, while accounting for the different human-robot sizes, we try to keep the normalized time derivative [4] of the DCMs identical:

$$\frac{\dot{\xi}_R}{\omega_R^\circ} = \frac{\dot{\xi}_H}{\omega_H} \tag{11}$$

where $\dot{\xi}_R = \dot{\theta}_R + \ddot{\theta}_R/\omega_R^\circ$ and $\dot{\xi}_H = \dot{\theta}_H + \ddot{\theta}_H/\omega_H$ are the time derivatives of the DCM in (6) and (8). This constraint 11 couples the angular dynamics of the human and robot as seen by expanding and substituting in (4) and (7):

$$\theta_R + \frac{\dot{\theta}_R}{\omega_R^\circ} - \frac{F_R}{\gamma_R} + \frac{F_{ext}}{\alpha^2\gamma_R} = \theta_H + \frac{\dot{\theta}_H}{\omega_H} - \frac{p_H}{h_H} + \frac{F_{HMI}}{\gamma_H} \tag{12}$$

where $\gamma_j = m_j\omega_j^2 h_j$ with $j = \{H, R\}$ has units Newtons and can be viewed as a nondimensionalizing scaling for human-robot forces. Although there are many choices of F_{HMI} and F_R that satisfy (12), we propose a specific formulation where the human's applied effort, captured by their CoP, is analogous to the force or effort applied on the robot cart-pole:

$$F_R = \frac{\gamma_R}{h_H} p_H \tag{13}$$

The robot force, F_R, captures the non-minimum phase behavior of the CoP and is particularly valuable for bi-wheeled humanoids as their base must also initially move in the opposite direction compared to the desired reference.

The remaining terms in (12) are fed back to the human to provide information about the robots states and interaction forces for an improved immersive experience:

$$F_{HMI} = \gamma_H \left((\theta_R - \theta_H) + \left(\frac{\dot{\theta}_R}{\omega_R^\circ} - \frac{\dot{\theta}_H}{\omega_H} \right) \right) + \frac{\gamma_H}{\alpha^2\gamma_R} F_{ext} \tag{14}$$

TABLE I
HUMAN-ROBOT MODEL PARAMETERS

Parameter	Symbol	Human	SATYRR	Units	Ratio
CoM Masses	m	52.0	12.6	kg	4.13
CoM Height	h	1.10	0.37	m	2.97
Natural Frequency	ω	2.99	5.15	s^{-1}	0.58
Upper Arm Length	l_A	0.31	0.18	m	1.72
Forearm Length	l_F	0.30	0.20	m	1.50
Base Masses	M	—	1.61	kg	—

More specifically, the feedback force tries to minimize the difference in the human-robot angular motions and also conveys the robot's external forces scaled by human-robot parameters.

A WIP Linear Quadratic Regulator (**LQR**), with controller states $[x_W, \dot{x}_W, \xi_R]^T$, is used to track the human DCM as shown in Fig. 3. To transfer the human's intended motion, improve responsitivity, and satisfy (12) (under perfect tracking), F_R is treated as a feedforward force. The resulting wheel control effort is given by:

$$\tau_W = -K_{LQR}(\xi_H - \xi_R) + F_R \tag{15}$$

Tracking of wheel position and velocity is intentionally disabled here as it can result in accumulation of error and wheel slip when interacting with unknown objects and forces e.g. pushing heavy boxes of unknown mass. Moreover, solely regulating the DCM allows the pilot to control interaction forces with the environment.

D. Virtual Spring Force

To allow the pilot to dynamically lean further without falling over, a safety force was incorporated as a virtual spring, $F_s = -K_s x_H$, where x_H is the human CoM displacement from their upright position. This is modeled by adding F_s/γ_H to both sides of (12). Here, $K_s = 400$ N/m is tuned by pilot preference. The resulting net feedforward and feedback terms are:

$$F_R \leftarrow F_R - \frac{\gamma_R}{\gamma_H} F_s \tag{16a}$$

$$F_{HMI} \leftarrow F_{HMI} + F_s \tag{16b}$$

The resulting haptic force, F_{HMI}, includes a virtual spring. Consequently, when the human leans forward, $F_s < 0$, the robot feedforward, F_R is also larger. This term encapsulates how much effort the human exerts to resist the spring. For box pushing, after the robot's lean and contact locations are chosen by the pilot, this augmented feedforward allows the robot to apply more effort via its wheels.

E. Kinematic Manipulation Retargeting

We leverage similarity in joint structure of the human and robot arms to create an intuitive kinematic mapping. Unlike the robot, the exosuit's shoulder axes do not intersect and are not spherical joints. Our approach aims to align the robot and human exosuit axes through inverse kinematics (**IK**).

We define the human exosuit and robot arm generalized coordinates: $\boldsymbol{q}^{(\cdot)} \in \mathbb{R}^4$ where the superscript H, R denote human exosuit and robot, whose coordinates q_0 to q_3 are joint angles as shown in Fig. 4 . The vector from human shoulder to elbow,

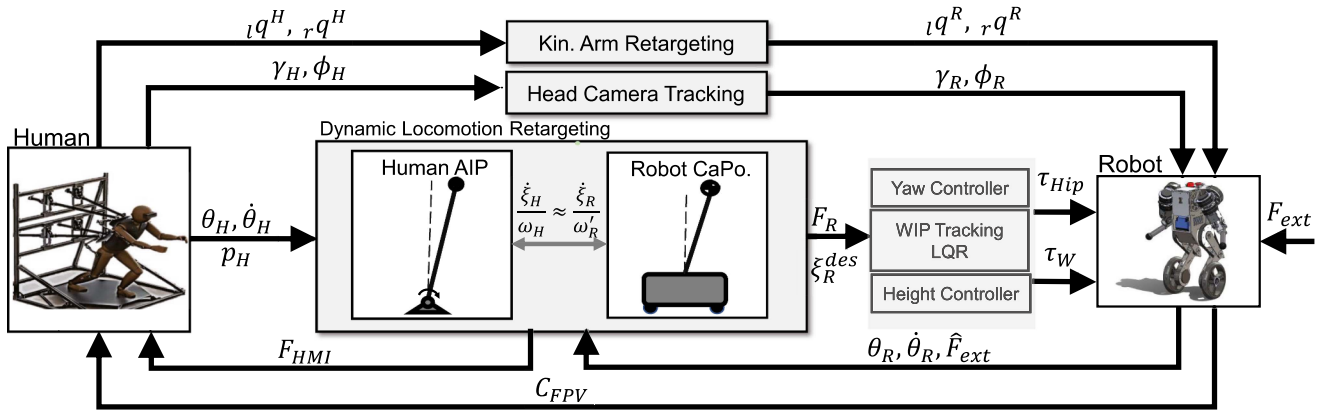

Fig. 3. Full system layout and bilateral teleoperation control framework. The real-time first-person view camera feedback is shown as C_{FPV}. The prescripts l, r represent the left and right hands. γ_H and ϕ_H represent the human head pitch and yaw.

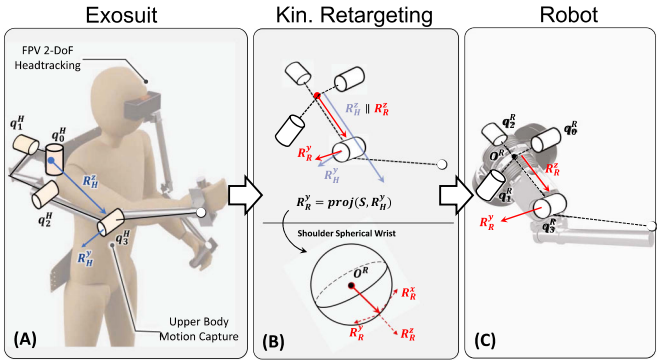

Fig. 4. Human arm motion is captured by an exosuit. A design choice was made to align the human-robot upper arm and elbow rotation axis in the shoulder spherical wrist mapping.

$\mathcal{R}_H^z \in \mathbb{R}^3$, in Fig. 4(a) can be found using the exosuit's forward kinematics.

We align the vector from the robot's shoulder to its elbow with the direction of the human's elbow ($\mathcal{R}_R^z = \mathcal{R}_H^z$) as seen in Fig. 4(b). To find the remaining axis we define the plane, $\mathcal{S}$, perpendicular to $\mathcal{R}_H^z$:

$$\mathcal{S} = \{\mathcal{R}_u \mid \mathcal{R}_u^\top \mathcal{R}_H^z = 0\} \tag{17}$$

The second axis of rotation can be subsequently set:

$$\mathcal{R}_R^y = \text{proj}_{\mathcal{S}}(\mathcal{R}_H^y) \tag{18}$$

The aim of this projection is to find the vector closest to that of the human elbow rotation axis $\mathcal{R}_H^y$ that is also perpendicular to the given $\mathcal{R}_H^z$ as shown in Fig. 4(b). The final axis is given by their cross product: $\mathcal{R}_R^x = \mathcal{R}_R^y \times \mathcal{R}_R^z$. With all 3 axes of the robot shoulder defined, we solve the inverse kinematics of the spherical wrist as given in [23]:

$$\boldsymbol{q}_{[0:2]}^R = \text{IK}(\mathcal{R}_R^x, \mathcal{R}_R^y, \mathcal{R}_R^z) \tag{19}$$

Similarity in human-robot joint structure leads to direct use of human elbow angle as reference for the robot: $q_3^R = q_3^H$.

The desired joint positions are sent to the motors, where an onboard tracking PD controller operates at 40 kHz:

$$\tau_{com} = K_p(q - q_{des}) + K_d(\dot{q} - \dot{q}_{des}) + \tau_{ff}$$

where $\tau_{ff} = 0$ and desired joint velocity are set to zero, $\dot{q}_{des} = 0$. By using proximal actuation design principles [24], lightweight limbs, and torque dense actuators with low-gear ratio transmissions as recommended in [25], we assume we can achieve agile end effector tracking at human reaction speeds without explicitly considering the arm's dynamics.

V. Experimental Setup

We conducted two experiments to showcase efficacy of the proposed mappings in whole-body teleoperation and DMM. The first set of experiments evaluate tele-locomanipulation tasks including standing in place, accurately tracking arm movements, and grabbing a moving object where the pilot simultaneously controls the robot's body and arms. Yaw control can be used in conjunction as done in [3] to enable 2D cartesian movement of the robot. Task 2 demonstrates a form of DMM where the pilot was required to push boxes between 4–13 kg at a constant velocity while keeping a bottle balanced on top of the box, as seen in Fig. 8. In this scenario, moving at a constant speed requires the pilot to regulate applied forces, while the bottle enforces bounds for the robot's acceleration. The pilot was unaware of the box's mass during these tests. In summary, success is determined not only by magnitude of force applied but also robot stability and a smooth motion profile. To highlight the effectiveness of the haptic feedback, F_{HMI}, this experiment is constrained to the sagittal plane using railings on the ground to prevent rotation of the box.

Due to the arm's design philosophy, as discussed in Section IV-E, the torques generated by contact greatly exceed the inertial torques. Therefore, we estimate the external force acting on the robot cart-pole by summing the contact forces at each hand:

$$\hat{F}_{ext} = \boldsymbol{\Lambda} \boldsymbol{J}_{c,r}^\dagger (\boldsymbol{G}\boldsymbol{\tau}_{m,r}) + \boldsymbol{\Lambda} \boldsymbol{J}_{c,l}^\dagger (-\boldsymbol{G}\boldsymbol{\tau}_{m,l}) \tag{20}$$

where r and l subscripts denote the right and left arm measured motor torque $\boldsymbol{\tau}_{m,(\cdot)} \in \mathbb{R}^4$, and Moore-Penrose inverse of the contact Jacobian, $\boldsymbol{J}_{c,(\cdot)}$. The motor-space to joint-space mapping matrix is given by $\boldsymbol{G} = blkdiag(-1, 1, 1, -2)$. The selection matrix, $\boldsymbol{\Lambda}$, isolates the x component of the contact force for the planar models considered in this work and we approximate the contact point height as the robot cart-pole height. Moreover, the contact at the end-effector implicitly captures friction forces,

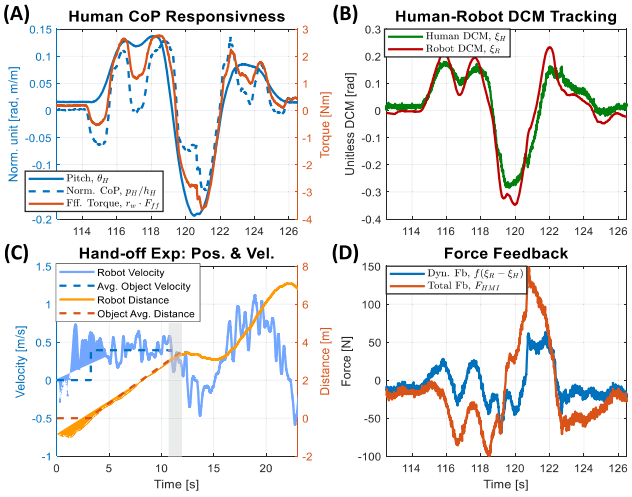

Fig. 5. Whole-body tele-locomanipulation results. (a) Highlights the non-minimum phase behavior of the CoP. (b) Shows the robot and human DCM tracking. (c) Shows the the dynamic hand off experiment where the robot starts at -0.75 m, and the box starts at -0.5 m. At $t = 11$ s, the robot catches up to the desired box position while traveling near the box's velocity. (d) Shows the dynamic feedback and net haptic feedback as the pilot leans.

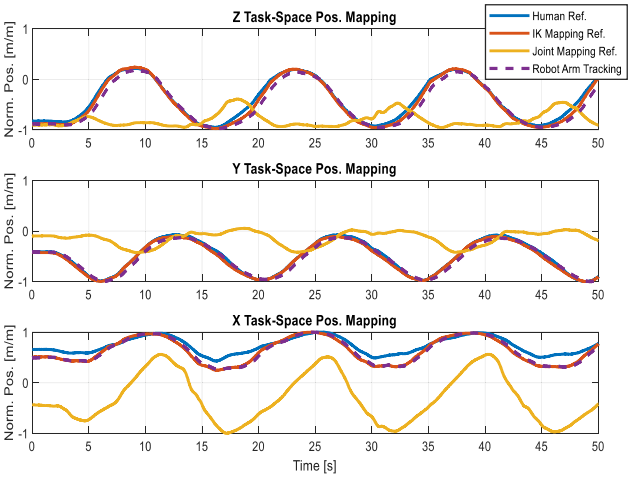

Fig. 6. Arm end effector mappings and tracking: the pilot moves their arm in a circular motion in front of their body. IK tracking was preferred.

reaction forces from the railings, and other disturbance forces that affect the box.

From previous experiments, we found that scaling of the external force helped the pilot better perceive interaction forces and was their preferred choice. Under perfect tracking, (14) and (16b) show that feedback to the human is dominated by the spring and external force. In this situation, to enable an immersive experience the haptic feedback should ideally convey the interaction force between the robot and the environment. Since the human is unable to perceive smaller changes in forces applied to their body, a scaled value of the estimated external force was used:

$$\hat{F}_{ext} \leftarrow K_{fb}\hat{F}_{ext} \tag{21}$$

The pilot's desire for perceiving a scaled interaction force preceded their desire for generating a dynamically consistent

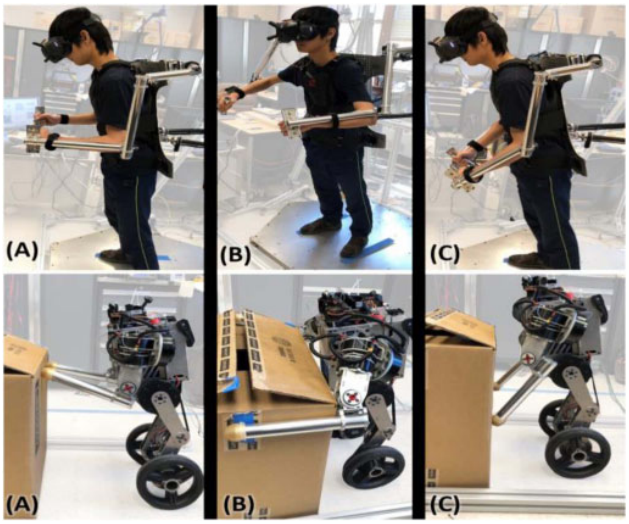

Fig. 7. Pilot tried different poses during box pushing experiments and adapted their strategy to move boxes weighing 8-13 kg (63.5-105% of m_R). In poses (a) and (b) the pilot was unable to push the box, but (c) was successful.

reference for the robot. While K_{fb} is intended to be constant, certain tasks may necessitate its modification that requires analysis beyond the scope of this study. Pilot tuning set $K_{fb} = 2.5$ for all experiments.

VI. Results & Discussion

Section VI-A discusses the first set of experiments that show whole-body teleoperation. Section VI-B shows the human-robot box pushing as a form of DMM. The experiments are conducted in compliance with the requirements from the UIUC Internal Review Board (IRB). Validation is shown on video.[1]

A. Whole-Body Tele-Locomanipulation Evaluation

While standing in place or moving, locomotion control benefits from using the human CoP as a feedforward as derived in Section IV-C. At $t = 115$ s in Fig. 5(a), we see how the CoP precedes human pitch movement and captures the non-minimum phase dynamics of human leaning when humans push off their heels to change pitch. This motion is a suitable feed-forward for the non-minimum phase robot, indicated by the initial $\tau_{ff} = -0.4$ Nm.

The DCM tracking of the human-robot can be seen in Fig. 5(b). As the robot controller tracks the human reference, ξ_H, the robot overshoots and briefly leads the human between time $t = 120 - 122$ s. We attribute this observed tracking behavior to three factors: indirect control of the robot's position through pitch, deviations from the idealized human model, and inherent dynamics differences due to the robot's smaller size. As seen in Fig. 5(d), the pilot is momentarily pushed forward at $t = 122$ s with a force of 50 N informing them of the robot's overshoot. While this feedback did not notably aid in stabilization, it did provide the pilot with situational awareness and an enhanced immersive experience by indicating the direction of disturbance forces acting on the robot's body. The pilot also tested two forms

[1][Online]. Available: https://youtu.be/QqcJsSH0YjY

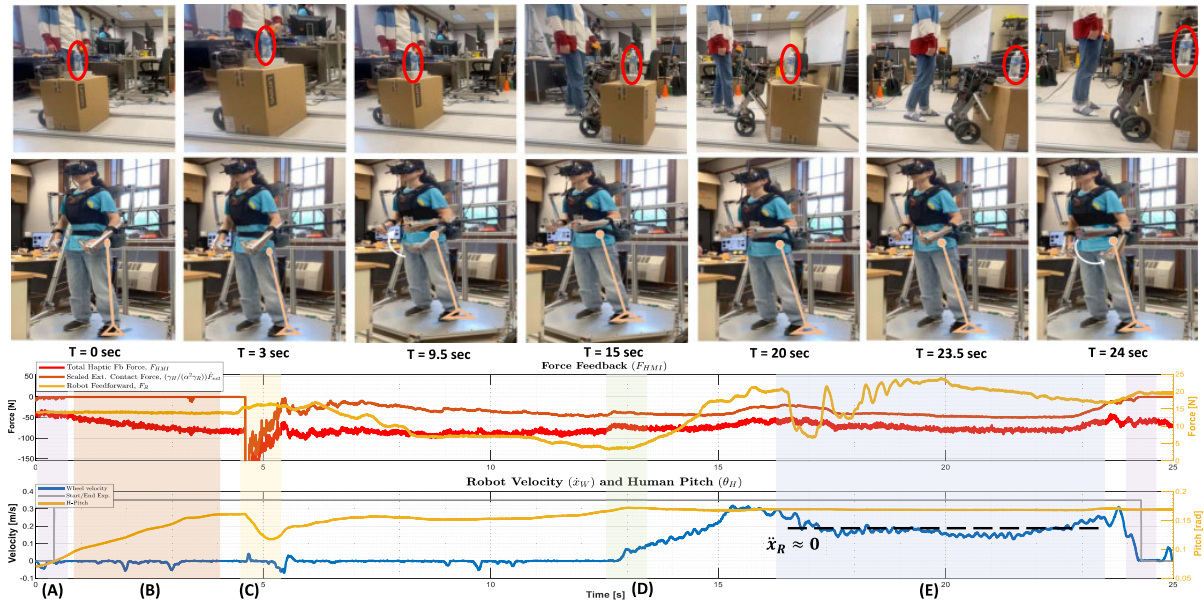

Fig. 8. Heavy box pushing experiment: A 8.5 kg (67.5 % of m_R) box with a balanced bottle is pushed at constant velocity. (a) Shows in purple start and end of task. In (b) the pilot initially increases their lean without using their arms. At (c) the robot's hands make contact with the box and begins pushing with the arms resulting in a sharp change in external contact force. The pilot continues moving their arms up until (d), where the robot breaks stiction and the box begins moving, accompanied by a change in external force. (e) shows the box moving at a constant velocity. At the end, the pilot breaks contact by lowering their hands. The right axis show the zoomed in feedforward force and human pitch in their respective graphs.

of arm mappings, where they preferred the IK mapping. As seen in Fig. 6 the IK mapping resulted in more accurate tracking of the human hand. The slight topological differences between the human arm, the exosuit that captured the humans motion, and the robot's arm were the driving factors in this choice. Moreover, the robot's proficient tracking of the IK mapping reference strengthens our approach of not explicitly modeling the robot arm dynamics when design principles from [25] are applied. Ultimately, this kinematic mapping proved to be intuitive for the pilot and enabled hands-free tele-manipulation.

Next, whole-body tele-locomanipulation was tested by requiring the robot to grab a moving package weighing 1.25 kg (10% of m_R). Completion of this task can be difficult as it requires estimation of object velocity. The the pilot was able to modulate the velocity to catch up to the moving package at $t = 11$ s, as shown in the grey region in Fig. 5(c). Without switching between locomotion and manipulation modes [17], the pilot was simultaneously able to command a desired arm motion for the robot to grab the object, pull it closer to its body to mitigate the moment created around its wheel, and complete the mobile hand-off. Visual feedback enabled the pilot to make grip adjustments, as shown in the supplementary task video.

B. Pushing Heavy Boxes: A Form of Whole-Body DMM

The experiments here require use of whole-body coordination to regulate and apply large forces on the environment. An initial adjustment of the robot pose was required to push heavier boxes. Finding an optimal pose for whole-body interaction and box pushing is a non-trivial task, requiring offline optimization [15]. By tracking the human DCM and arm movement, the robot's stance can be adjusted on the fly as seen in Fig. 7. The final chosen pose shown in Fig. 7(c) maximized the achievable lean of the robot while keeping its hands closer to the bottom of the box—much like a human might. Without this modification, the robot was unable to push boxes greater than 8 kg. This adaptation highlights the effectiveness of leveraging human planning for DMM.

Fig. 8 shows the pilots whole-body strategy for pushing the 8.5 kg box at a constant velocity. After starting the trial run indicated by the grey line in Fig. 8, the pilot increases their lean on the box between $t = 1$ s and $t = 4$ s. At $t = 4.5$ s, the box has not moved and the pilot telemanipulates the robot hands to begin pushing on the box. This initially results in a sharp change in contact forces as seen in Fig. 8(c). Force estimation using joint torques is particularly susceptible to noise when the contact point velocity is nonzero. Between $t = 5$ s and $t = 13$ s, the pilot maintains their lean and slowly moves their arms to increase the applied force as seen by the increase in $|\hat{F}_{ext}|$. This upward arm motion also momentarily lifts the front of the box. We believe this helped in breaking static friction forces between the box and ground to start the box's movement as shown in green in Fig. 8(d). As the robot-box move at a constant velocity ($\dot{x}_R \approx 0.2$ m/s) as highlighted in the blue section of the figure, the feedback forces are nearly constant — $F_{HMI} \approx -80\,N$. Upon crossing the finish line, the pilot stops by putting their hands down.

Haptic forces played a pivotal role in completing the box pushing task, encompassing three components: dynamic feedback, external force feedback, and spring force. The dynamic feedback provided information to the pilot regarding the balance of the robot, as well as the direction of disturbances on the robot's body. The external force feedback informs the pilot of the end effector contact force, which captures unmodeled forces on the box. This

gives the pilot opportunities to adjust their locomotion strategy in response to variations in box weight, friction conditions, and railing contact. The pilot found the spring feedback force most useful, as it allowed for comfortable extended leaning due to its predictable response.

Without haptic feedback, i.e. $F_{HMI} = 0$ and $F_s = 0$, the pilot was unable to push the box. We believe this is because the pilot could not lean as far and there was less feedforward, as described in (16a), to help break stiction. Based on empirical observations, applying enough force to break stiction was the bottleneck in getting the box to move. Under the same bilateral teleoperation framework, various other feedback laws can be implemented based on (12), offering different haptic experiences and responses from the pilot.

C. Limitations

Generating position-velocity trajectories without box weight or friction knowledge is challenging. Prior work [3] resulted in accumulated error and wheel slip when dealing with external forces ($x_w^{des} = \iint g\theta_H(t)dt$). Thus, we did not track position but had the pilot control acceleration by modulating the robot's pitch, making it challenging to maintain a stationary position.

Through extensive testing, our pilot could interpret the force feedback but faced challenges in discerning finer details, likely due to limited feedback resolution at the human CoM. This presents a potential obstacle for future whole-body bilateral teleoperation, as the dynamic feedback signal at the CoM is not easily utilized for precise regulation. Providing feedback to the user's hand could address this problem as the hand has high force-sensing resolution. Moreover, to generalize how humans perceive the feedback forces and use it to inform their decision making in the context of DMM whole body teleoperation, a larger pilot study is needed. Overall, our experiments showed that humans excel as motion planners.

VII. Conclusion

In this letter, we presented a framework to perform DMM via whole-body bilateral teleoperation. The locomotion mapping models external forces on the robot and utilizes the human's balancing strategy captured by their AIP DCM to generate tracking references. An IK arm mapping enables the pilot to manipulate simultaneously. Finally, through box pushing experiments, we show how the pilot-robot can regulate applied forces on the environment using their body and arms. Human force feedback facilitates dynamic leaning motions and perception of interaction forces between the environment and robot. In future work, we aim to integrate advanced grippers and force sensors to demonstrate pulling and lifting behaviors.

Acknowledgment

The authors would like to thank their colleagues Youngwoo Sim, Guillermo Colin, and Donghoon Baek for their guidance throughout this work.

References

[1] L. Penco et al., "Robust real-time whole-body motion retargeting from human to humanoid," in *Proc. IEEE-RAS 18th Int. Conf. Humanoid Robots*, 2018, pp. 425–432.

[2] A. Dallard, M. Benallegue, F. Kanehiro, and A. Kheddar, "Synchronized human-humanoid motion imitation," *IEEE Robot. Automat. Lett.*, vol. 8, no. 7, pp. 4155–4162, Jul. 2023.

[3] A. Purushottam, Y. Jung, K. Murphy, D. Baek, and J. Ramos, "Hands-free telelocomotion of a wheeled humanoid," in *Proc. IEEE/RSJ Int. Conf. Intell. Robots Syst.*, 2022, pp. 8313–8320.

[4] J. Ramos and S. Kim, "Humanoid dynamic synchronization through whole-body bilateral feedback teleoperation," *IEEE Trans. Robot.*, vol. 34, no. 4, pp. 953–965, Aug. 2018.

[5] S. Wang and J. Ramos, "Dynamic locomotion teleoperation of a reduced model of a wheeled humanoid robot using a whole-body human-machine interface," *IEEE Robot. Automat. Lett.*, vol. 7, no. 2, pp. 1872–1879, 2022.

[6] J. Cheng, F. Abi-Farraj, F. Farshidian, and M. Hutter, "Haptic teleoperation of high-dimensional robotic systems using a feedback MPC framework," in *Proc. IEEE/RSJ Int. Conf. Intell. Robots Syst.*, 2022, pp. 6197–6204.

[7] M. Risiglione, J.-P. Sleiman, M. V. Minniti, B. Cizmeci, D. Dresscher, and M. Hutter, "Passivity-based control for haptic teleoperation of a legged manipulator in presence of time-delays," in *Proc. IEEE/RSJ Int. Conf. Intell. Robots Syst.*, 2021, pp. 5276–5281.

[8] A. Dietrich, T. Wimböck, and A. Albu-Schäffer, "Dynamic whole-body mobile manipulation with a torque controlled humanoid robot via impedance control laws," in *Proc. IEEE/RSJ Int. Conf. Intell. Robots Syst.*, 2011, pp. 3199–3206.

[9] G. Zambella et al., "Dynamic whole-body control of unstable wheeled humanoid robots," *IEEE Robot. Automat. Lett.*, vol. 4, no. 4, pp. 3489–3496, Oct. 2019.

[10] H. Zhou, X. Li, H. Feng, J. Li, S. Zhang, and Y. Fu, "Model decoupling and control of the wheeled humanoid robot moving in sagittal plane," in *Proc. IEEE-RAS 19th Int. Conf. Humanoid Robots*, 2019, pp. 1–6.

[11] G. Colin, Y. Sim, and J. Ramos, "Bipedal robot walking control using human whole-body dynamic telelocomotion," in *Proc. IEEE Int. Conf. Robot. Automat.*, 2023, pp. 12191–12197.

[12] M. V. Minniti, R. Grandia, K. Fäh, F. Farshidian, and M. Hutter, "Model predictive robot-environment interaction control for mobile manipulation tasks," in *Proc. IEEE Int. Conf. Robot. Automat.*, 2021, pp. 1651–1657.

[13] M. Stilman, J. Olson, and W. Gloss, "Golem Krang: Dynamically stable humanoid robot for mobile manipulation," in *Proc. IEEE Int. Conf. Robot. Automat.*, 2010, pp. 3304–3309.

[14] M. Mittal, D. Hoeller, F. Farshidian, M. Hutter, and A. Garg, "Articulated object interaction in unknown scenes with whole-body mobile manipulation," in *Proc. IEEE/RSJ Int. Conf. Intell. Robots Syst.*, 2022, pp. 1647–1654.

[15] S. Caron, "Divergent components of motion," in *Proc. JRL Seminar*, 2019. [Online]. Available https://scaron.info/slides/jrl-2019.pdf

[16] Y. Wu, P. Balatti, M. Lorenzini, F. Zhao, W. Kim, and A. Ajoudani, "A teleoperation interface for loco-manipulation control of mobile collaborative robotic assistant," *IEEE Robot. Automat. Lett.*, vol. 4, no. 4, pp. 3593–3600, Oct. 2019.

[17] N. E. Sian, K. Yokoi, S. Kajita, F. Kanehiro, and K. Tanie, "Whole body teleoperation of a humanoid robot development of a simple master device using joysticks," *J. Robot. Soc. Jpn.*, vol. 22, no. 4, pp. 519–527, 2004.

[18] K. Otani and K. Bouyarmane, "Adaptive whole-body manipulation in human-to-humanoid multi-contact motion retargeting," in *Proc. IEEE-RAS 17th Int. Conf. Humanoid Robot.*, 2017, pp. 446–453.

[19] Y. Ishiguro et al., "Bilateral humanoid teleoperation system using whole-body exoskeleton cockpit TABLIS," *IEEE Robot. Automat. Lett.*, vol. 5, no. 4, pp. 6419–6426, Oct. 2020.

[20] R. A. Grupen, "Putting it all together: Balancing the cart-pole," Dept. Comput. Sci., Univ. Massachusetts, Amherst, MA, USA, Tech. Rep. 1, 2015. [Online]. Available: https://www-robotics.cs.umass.edu/grupen/503/SLIDES/cart-pole.pdf

[21] A. Hof, M. Gazendam, and W. Sinke, "The condition for dynamic stability," *J. Biomech.*, vol. 38, no. 1, pp. 1–8, 2005.

[22] S. Caron, "Divergent components of motion," 2019. [Online]. Available: https://scaron.info/slides/jrl-2019.pdf

[23] S. Asif and P. Webb, "Kinematics analysis of 6-DoF articulated robot with spherical wrist," *Math. Problems Eng.*, vol. 2021, 2021, Art. no. 11.

[24] Y. Sim and J. Ramos, "Tello leg: The study of design principles and metrics for dynamic humanoid robots," *IEEE Robot. Automat. Lett.*, vol. 7, no. 4, pp. 9318–9325, Oct. 2022.

[25] S. Seok et al., "Design principles for energy-efficient legged locomotion and implementation on the mit cheetah robot," *IEEE/ASME Trans. Mechatron.*, vol. 20, no. 3, pp. 1117–1129, Jun. 2015.